ADVANCED MATERIALS INTERFACES

www.advmatinterfaces.de

Supersonically Sprayed Copper–Nickel Microparticles as Flexible and Printable Thin-Film High-Temperature Heaters

Jong-Gun Lee, Do-Yeon Kim, Tae-Gun Kim, Jong-Hyuk Lee, Salem S. Al-Deyab, Hyun Woo Lee, Jang Soo Kim, Dae Ho Yang, Alexander L. Yarin, and Sam S. Yoon**

Cu and Ni nanoparticles are sprayed at supersonic velocities onto stiff glass, ceramic, and marble surfaces, as well as onto flexible polymer substrates of complex shapes. Joule heating occurs when a voltage is applied to the sprayed Cu–Ni thin films, enabling their use as thin-film heaters. The Cu–Ni composition is varied to control the electrical and the thermal properties of the films, which affects the total amount of power used for the heating. At a high Cu content, the temperature reaches as high as 1000 °C, which significantly broadens the range of potential applications of such film heaters. The thermal stability of the film heaters is confirmed by cyclic testing, which shows repeatable rapid undulations in the temperature range of 600 °C. The Cu–Ni film heaters can be printed on any type of substrates including mirrors, glasses, and flexible polymers, and the method of film fabrication is rapid and scalable. The surface temperature of the heater is measured experimentally and matches well with the theoretical predictions. The Cu–Ni film heaters find applications in vehicle defrosters, smart heat-retaining windows, domestic appliances, etc., and industrial heating and defrosting of complex surfaces.

1. Introduction

Heaters are widely used for both domestic and industrial applications. Some examples of the domestic uses are electric heating systems for houses, heated seats in automobiles, toasters, cooking wares, and water boilers.[1,2] The industrial applications are countless since almost all thermal engineering systems use heaters to sustain their manufacturing processes. In particular, high-performance transparent heaters are of interest for various applications including solar cell panels, vehicle defrosters, and smart heat-retaining windows exposed to cold and icy conditions.[3–13] The public demand for aesthetically pleasing home appliances such as transparent toasters, water heaters,[14] and portable air heaters is another driving force for the development of transparent heaters. Often, these heaters need to be installed in curved or complex shapes such as those found in heated clothing, shoes, and gloves. The heating of curved shapes necessitates the use of curved or flexible heaters.

Flexible transparent conducting films have been extensively developed in the last few years using nanomaterials such as carbon nanotubes (CNTs),[15–18] graphene,[19–21] Ag nanowires,[22–28] metal grids,[29–32] nanofibers,[33–35] and nanoparticles.[36,37] Although the use of nanomaterials enables high transparency and low material consumption, the applications of nanomaterial-based heaters are limited to low temperatures. This is because the nanomaterial-based heaters can sustain only limited power supply levels, beyond which malfunctions such as wire melting and electrostatic shocks can occur.[38] In general, the temperature ranges for the operation of CNT, graphene, and Ag nanowire-based heaters are 77–160,[15–18] 100–206,[19–21] and 48–160 °C,[22–25,27,28] respectively. A heater utilizing a hybrid material of graphene and Ag nanowires was found to achieve a maximum temperature of 230 °C.[39] However, these temperature ranges are insufficiently high for industrial applications such as hot stamping,[40] and others which require operating temperature as high as ≈1000 °C.[41,42] The surface temperature (T_s) of a heater is governed by the amount of supplied electric power (P); $T_s \sim P$, and $P = V^2/R$, where V is the supplied voltage and R is the resistance of the heating material. To reduce R, a larger cross-sectional (to the electric current direction) area (A) must be used, since $R = \rho_s L/A$, where, L and ρ_s are the length and the specific resistivity of a heating material, respectively. In this respect, nanomaterials are not preferable because they have small cross-sectional areas. Therefore, nanomaterials with low ρ_s have been used to

J.-G. Lee, D.-Y. Kim, T.-G. Kim, J.-H. Lee, Prof. S. S. Yoon
School of Mechanical Engineering
Korea University
Seoul 02841, Republic of Korea
E-mail: skyoon@korea.ac.kr
Prof. S. S. Al-Deyab
Petrochemicals Research Chair
Department of Chemistry
King Saud University
Riyadh 11451, Saudi Arabia
H. W. Lee, J. S. Kim, D. H. Yang
MS AUTOTECH
1023, Nogokli, Nanamyun, Gyungju 780-851, Republic of Korea
Prof. A. L. Yarin
Department of Mechanical and Industrial Engineering
University of Illinois at Chicago
842 W. Taylor St., Chicago, IL 60607-7022, USA
E-mail: ayarin@uic.edu

DOI: 10.1002/admi.201700075

compensate for the small *A* and accommodate ample supplies of power.

A 2D film-type heating material is a good compromise, providing a reasonable cross-sectional area and conductivity for a given power level in domestic uses. Such 2D film heaters often need to be installed on curved surfaces, which is challenging because of the adhesion-related issues. Furthermore, the complex design or patterning requirements for aesthetic purposes complicate the process of heater fabrication. 1D metal grids are usually patterned with Ag ink or paste, using inkjet or screen-printing techniques.[29–32,43] However, it is extremely difficult to fabricate 2D film heaters using such techniques.

In this work, a supersonic cold spraying technique was used for the fabrication of 1D metal grids and 2D film heaters using Cu–Ni particles for applications at extremely high temperatures (>≈600 °C). Supersonic cold spraying allows deposition of electrically conducting materials on surfaces with any topography. The Cu–Ni particles were used in the present study as they are low-cost materials, and they could be deposited on various substrates. Patterning was carried out using a patterned mask, and the heating of patterned lines and letters has been demonstrated. The deposition method used in this study is rapid and scalable and the resistance of the heater can be easily tuned by changing the composition of the metallic film. The Cu–Ni particles were coated by the spraying technique on a 5 cm tall replica of the Jeju's Dol Hareubang statue in 30 s, demonstrating the potential for rapid mass production.

2. Results and Discussion

The scanning electron microscope (SEM) images of the Cu and the Ni particles are shown in the insets in **Figure 1**a. The particle size distribution of the Cu–Ni powder with a composition of 5:5 appears to be bimodal, as shown in Figure 1a. The particle size of Cu ranges from a few to some tens of micrometers ($D_{p,avg}$ = 6 µm), while that of Ni ranges from a few micrometers to less than 1 µm ($D_{p,avg}$ = 1.64 µm). Since the Ni particles are much smaller than the Cu particles, Ni can mix easily into the Cu particles while flattening during the supersonic impact. Owing to the ductile nature of the metallic particles, they do not undergo fragmentation or pulverization. On the contrary, the particles undergo an elastic-plastic deformation while flattening, resulting in the formation of distinct grain boundaries around each particle or cluster. These particles often arrive at the substrate as a cluster despite being dispersed in a solution precursor and sonicated using an atomizer prior to the injection into the supersonic stream. The deposited clusters may be further pulverized by the bombardment of the incoming particles.

The X-ray diffraction (XRD) patterns of the Cu–Ni composite powder and the film are shown in Figure 1b. The diffraction peaks observed at 43.3°, 50.5°, and 74.1° for the Cu powder, and 44.5°, 51.9°, and 76.4° for the Ni powder correspond to the (110), (200), and (220) planes of the fcc structures of Cu and Ni, respectively. Both the Cu–Ni powder and the film exhibit the characteristics

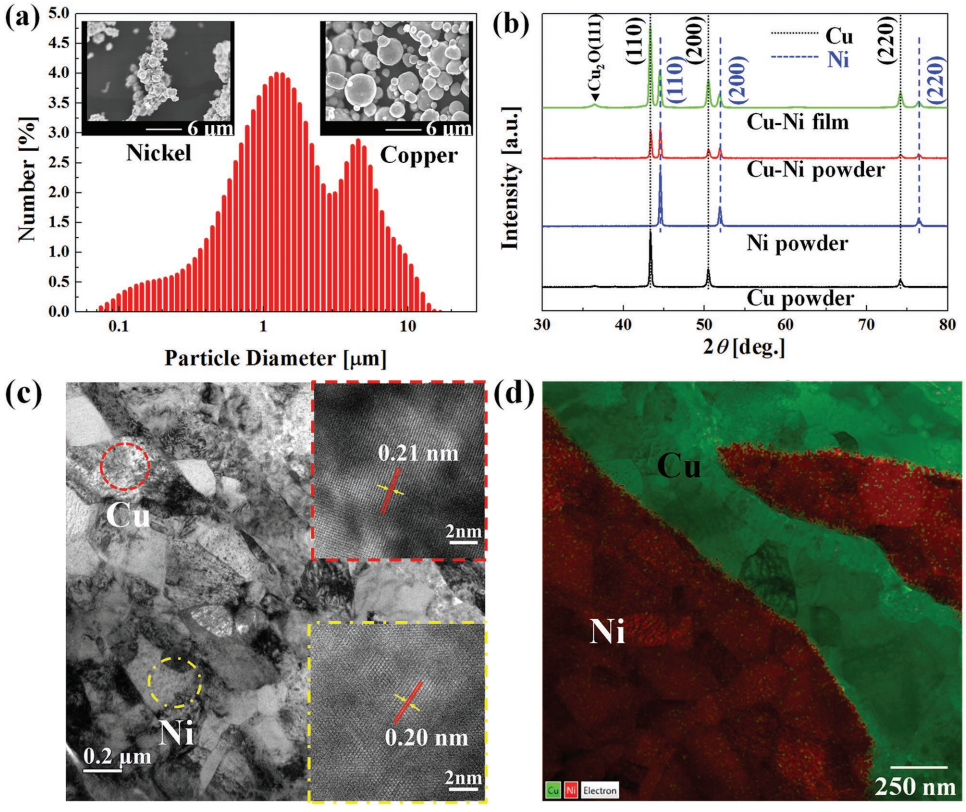

Figure 1. a) Particle-size distribution of the Cu–Ni particle mixture (5:5) and SEM images of the Ni and the Cu particles (insets). b) XRD patterns of Cu, Ni, Cu–Ni mixture (powder), and the supersonically deposited Cu–Ni film. c) Low-magnification TEM image of the Cu–Ni composite film. High-resolution TEM images of the Cu and the Ni particles are shown in the insets. d) EDX image of the cross–section of the supersonically sprayed Cu–Ni film. The number of sweeps was fixed at *N* = 20.

of both Cu and Ni, confirming the inclusion of both metals in the film. However, a minor peak corresponding to Cu_2O was observed in the film pattern, because of the local sintering and oxidation caused by the supersonic impact during spray coating.

Figure 1c shows the transmission electron microscopy (TEM) image of the Cu–Ni composite film produced at a pressure of $P_0 = 4$ bar and a temperature of $T_0 = 650$ °C. The TEM sample was prepared using focused ion beam (FIB) milling. The low-magnification TEM image confirms the presence of both Cu and Ni in the film. The film is composed of discrete Cu and Ni particles, which is clearly evident from the grain boundaries between the particles. The insets in Figure 1c depict the high-resolution TEM (HRTEM) images of the Cu (upper inset) and Ni (lower inset) particles in the regions marked by the red and yellow circles, respectively. The lattice plane spacing of Cu is 0.21 nm, which corresponds to the (111) plane at $2\theta = 43.3°$ observed in the XRD data and that of Ni is 0.20 nm, which corresponds to the (111) plane at $2\theta = 44.5°$.

Figure 1d shows the energy-dispersive X-ray spectroscopy (EDX) image of the Cu–Ni film deposited onto an alumina substrate. The top layer of the sample (shown in Figure 1d) was coated with platinum prior to FIB milling, to acquire the cross-sectional view of the sample. In the TEM image, the Ni particles appear darker than the Cu particles, although some Cu particles are darker than Ni. Their composition was identified by EDX.[44] In the EDX image of Figure 1d, the dark red and the green domains represent the Ni and the Cu particles, respectively. The weight ratio of the mixture in the cross–section was found to be ≈4.8:5.2, which nearly matches the initial weight ratio of 5:5 in the mixture. Although the interface between Cu and Ni is clearly distinct, its appearance confirms strong adhesion between the layers, promoted by the self-adhesion phenomenon that occurs during the supersonic cold spraying.[44]

Cu–Ni films with different compositions (weight ratios of Cu:Ni) were also deposited and the values of their resistance are listed in Table S2 (Supporting Information). The heaters fabricated using these films can be operated at high surface temperatures, as shown in **Figure 2**. The steady-state surface temperature is calculated using the following 1D thermal balance equation that accounts for the heat losses due to natural convection (buoyancy-driven flow) and radiation

$$P = hA(T_s - T_\infty) + \varepsilon\sigma A(T_s^4 - T_\infty^4) \tag{1}$$

where P is the supplied power, h is the heat transfer coefficient, A is the area over which heat transfer occurs, T_s is the surface temperature, T_∞ is the air temperature far from the heater surface, ε is the surface emissivity, and σ is the Stefan–Boltzmann constant ($\sigma = 5.67 \times 10^{-8}$ W m^{-2} K^{-4}). Equation (1) is transformed to the following dimensionless quartic equation

$$\overline{T_s}^4 + D\overline{T_s} - E = 0 \tag{2}$$

where the dimensionless groups D and E are defined as

$$D = \frac{h}{\varepsilon\sigma T_\infty^3}, \quad E = 1 + D + \frac{P}{\varepsilon\sigma A T_\infty^4} \tag{3}$$

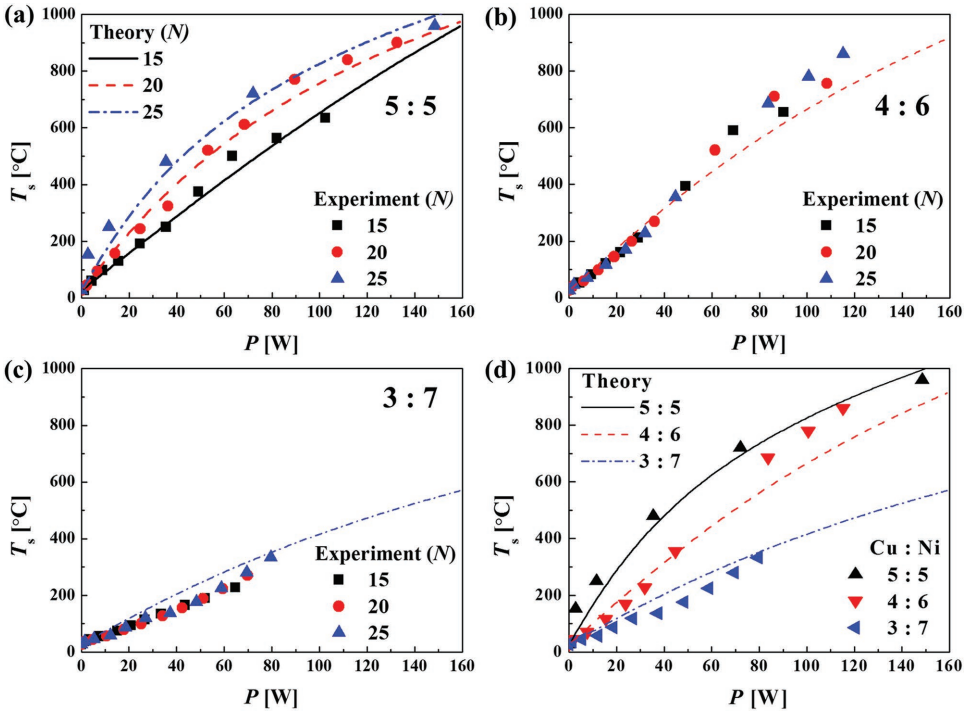

Figure 2. Effect of number of nozzle sweeps (N) on the surface temperature of the heaters with Cu:Ni ratio of a) 5:5, b) 4:6, and c) 3:7. d) The variation in the surface temperature at different weight ratios of Cu:Ni at a fixed value of $N = 25$. The experimental data are presented by symbols and the theoretical predictions are shown by curves. Air temperature of $T_\infty = 27$ °C (or 300 K) and heat transfer coefficient of $h = 100$ W K^{-1} m^{-2} were used for the calculations.

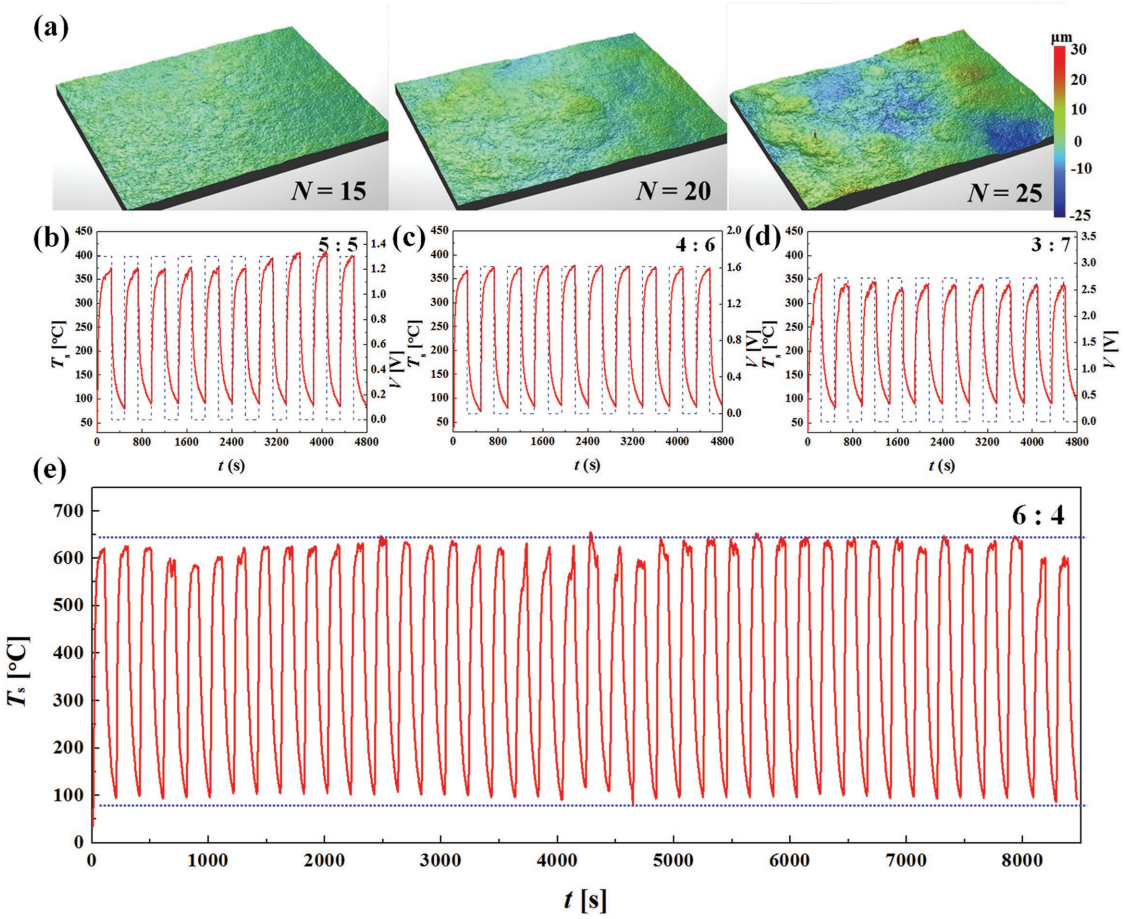

Figure 3. a) Optical profiler images of the cold-sprayed Cu–Ni films at $N = 15$, 20, and 25 at Cu:Ni ratio of 5:5. b–d) Results of the cyclic thermal stability test for the films fabricated at Cu:Ni weight ratios of 5:5, 4:6, and 3:7, respectively, for ten cycles. e) Cyclic thermal stability test for a film of Cu:Ni with a weight ratio of 6:4 for 42 cycles. The number of sweeps was fixed at $N = 20$ for the test data presented in (b)–(e).

and the dimensionless surface temperature is defined as $\overline{T_s} = T_s/T_\infty$.

In Equation (2), starting from the left-hand side, two coefficients of the polynomial are positive (namely, 1 and D), while the next one (the third one: $-E$) is negative. Therefore, the signs of the coefficients change only once, and according to the Descartes' rule of signs,[45] Equation (2) has a single real positive root, which is the only relevant root in the present case on physical grounds.

The theoretically predicted values of the surface temperature are compared to the experimentally measured ones in Figure 2. It should be noted that the thermocouple temperature was recorded at five different axial locations, whose averaged values are presented in Figure 2. In the predictions of the effect of N (the number of nozzle sweeps) on the surface temperature, T_s in **Figure 3**a, the emissivity value of $\varepsilon = 0.78$ corresponding to copper oxide (the most dominant particles in the Cu–Ni mixture with Cu:Ni ratio of 5:5 at all values of N) was used. The values of the effective surface area were $A = 13$, 10, and 8 cm^2 for $N = 15$, 20, and 25, respectively, which indicate that the surface roughness decreases at higher values of N. The decrease in the surface area with increase in N is discussed later along with the data on the dependence of surface roughness on N presented in Figure 3a. In the data presented in Figure 2d, the values of the surface emissivity and the area were varied as $\varepsilon = 0.78$, 0.9, and 0.9 and $A = 8$, 10, and 13 cm^2 to account for the increasing content of Ni at the surface for Cu:Ni = 5:5, 4:6, and 3:7, respectively, and the value of N was fixed at 25. The increase in the value of ε at a fixed value of $N = 25$ with an increased content of nickel oxide at the surface is associated with the fact that the emissivity of an oxidized nickel surface ($\varepsilon = 0.9$) is higher than that of oxidized copper ($\varepsilon = 0.78$). Accordingly, the surface temperature of an oxidized nickel surface is lower than that of an oxidized copper surface. This conduced to the increase in the surface temperature with an increase in the copper content on the surface as revealed by the experimental data in Figure 2d. It should be emphasized that the higher the nickel content, the weaker is the dependence of the surface temperature on N. This is because the tiny nickel particles would have already achieved the final value of roughness at $N = 15$.

Figure 3a shows the optical profiler images of the cold-sprayed Cu–Ni films fabricated at different values of N. The roughness values are listed in Table S3 (Supporting Information), where R_a, R_q, and R_t are the arithmetic average, root mean squared, and maximum height roughnesses,

respectively. It is clear that the surface roughness increases with increase in the value of N. On the other hand, the results related to Figure 2 showed that the surface area decreases as N increases. This situation seems to be paradoxical, since the decrease in the surface area is accompanied by an increase in the roughness as N increases. However, in the case of polydisperse particles such as those of Cu and Ni (cf. the SEM images in the insets in Figure 1a), this behavior is possible, as shown by the example demonstrated in detail in the Supporting Information. It should be emphasized that the losses due to both natural convection and radiation are proportional to the surface area, A. Equation (1) shows that if A decreases at a fixed supplied power P, the surface temperature T_s inevitably increases.

Figure 3b–d shows the time-dependent variation in the surface temperature (T_s) for the Cu:Ni compositions of 5:5, 4:6, and 3:7, respectively. The voltage supply was altered at an interval of 480 s for ten cycles, comprising a total time of 4800 s. In Figure 3b–d, the T_s and the applied voltage are shown on the vertical axes. It is shown that a higher voltage level was required for the heater with a lower Cu content to achieve the same surface temperature due to the higher value of resistance as shown in Table S2 (Supporting Information) and in accordance with $P = V^2/R$. For example, for the Cu:Ni ratio of 5:5 in (b), the voltage required to reach T_s of ≈400 °C was about 1.2 V, whereas for the ratio of 3:7 in (d), the voltage required to reach T_s of ≈350 °C was about 2.75 V. In summary, the applied voltage was maintained at 1.3, 1.6, and 2.75 V for the Cu:Ni ratios of 5:5, 4:6, and 3:7, respectively. All the films responded rapidly to the variation in the applied voltage with sharp undulations in the surface temperature, which reveals the high performance of the fabricated film heaters. This cyclic test for T_s is highly repeatable, with no signs of degradation while achieving $T_{s,max}$ for $t > 4800$ s. These results demonstrate the good thermal stability of the films when the maximum temperature of the cyclic test is maintained below 420 °C. Figure 3e shows the successful thermal cyclic test up to 42 cycles for a Cu:Ni film fabricated at the weight ratio of 6:4. The applied voltage was ≈1.3 V and T_s greater than 600 °C was achieved.

Figure 4 demonstrates the patterning capacity of the supersonic cold spraying method on both rigid glass and flexible polymer substrates. Lines of various thicknesses were deposited on a glass substrate as shown in Figure 4a and the thermal responses are shown by the infrared (IR) image in the inset. A flexible film heater is shown in Figure 4b. The film was connected to a light-emitting diode (LED) to demonstrate the conducting nature of the flexible printed line. The bendable printed line was attached to a voltage source and the temperature quickly increased to 95 °C (the IR image), revealing the high performance of the fabricated heater. This type of flexible and printable heater can be used in various applications such as vehicle defrosters in cold environments.

Figure 4c shows a 2 mm thick freestanding Cu–Ni thin film fabricated at $N = 30$. This film was made by spraying Cu–Ni particles onto an alumina substrate, and then detached from the substrate. The film was fixed at both sides using supports before the voltage was applied, as shown in Figure 4d. The film undergoes Joule heating, and the temperature rises as high as 1000 °C, which is the average temperature of five different thermocouple data at various axial locations. The film turns red hot and buckles because of the thermal expansion, as evident from the photograph. When the film was heated without detaching from the alumina substrate, the same thermal expansion occurred which eventually broke the substrate. The breaking of the alumina substrate demonstrates the excellent adhesion of the film to the substrate. The film was not delaminated from the substrate under tension and buckling resulting from the thermal expansion, which manifests an excellent bonding and adhesion to the substrate.

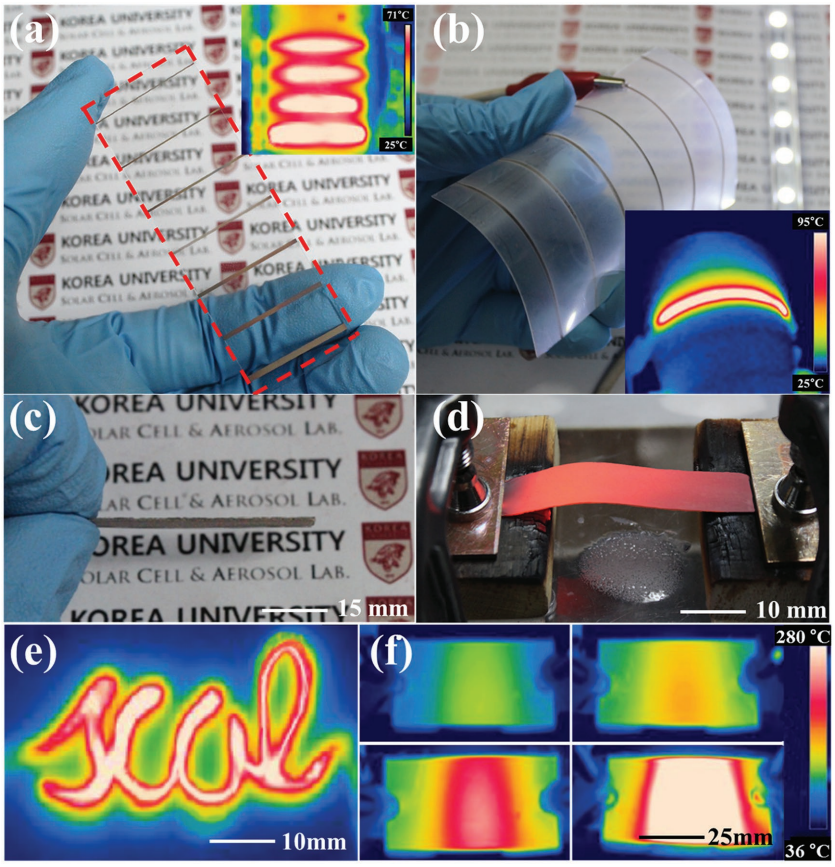

Figure 4. Photographs of the line patterns coated on a) a rigid glass and b) a flexible polyethylene terephthalate substrate; the insets show the corresponding IR image. The LED is seen in the background in (b). Photographs showing c) a Cu:Ni thin film and d) the Cu:Ni thin film undergoing Joule heating under an applied voltage. IR images of e) the letters "scal" patterned with Cu:Ni particles on an alumina substrate and subsequently heated, and f) a 2D planar film heater heated up to 280 °C. The scale bar is 25 mm and the temperature scale is the same for (e) and (f). The Cu:Ni weight ratio was 5:5.

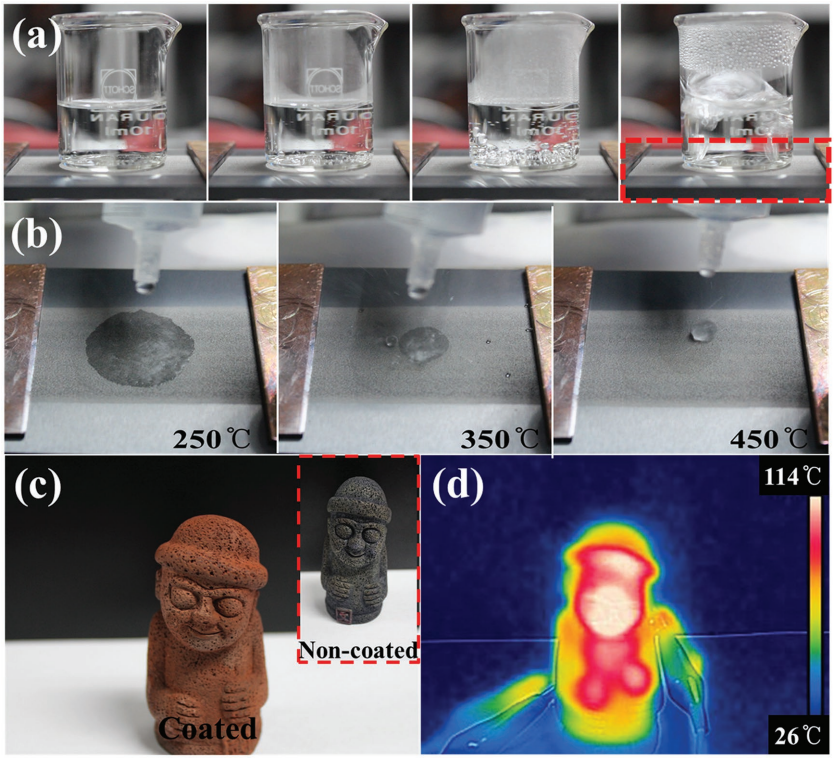

Figure 5. a) Gradual heating of a beaker of water placed on a Cu–Ni coated alumina substrate at the applied voltage of 1 V. The number of nozzle sweeps for this film was $N = 10$. b) Behavior of water drops placed onto the heater surface maintained at different temperatures (250, 350, and 450 °C). c) A Hareubang statue replica coated with Cu–Ni particles. d) IR image of the Hareubang statue after the onset of heating.

Figure 4e demonstrates the printing capability of the supersonic spray coating method. A stainless steel mask with the printed cursive letters "scal" in a hollow form was first machined. Then, the Cu–Ni particles were sprayed directly onto the mask, so that only the letters were printed. Figure 4f shows the gradual heating of a Cu–Ni film printed on an alumina substrate. When a voltage is applied, the center radiates first, then the high-temperature domain propagates sideways, and eventually most of the 2D surface is heated. It should be emphasized that a large surface area requires a high power to reach a high surface temperature.

Figure 5a,b shows the gradual heating of a beaker of water placed on the Cu–Ni film heater coated on an alumina substrate with $N = 10$, which yielded a film of thickness less than ≈1 mm. The substrate temperature reaches $T_s = 300$ °C within 30 s of the Joule heating, cf. panel (a) and then, boiling sets in. This is most apparent in the image on the extreme right corresponding to $t = 120$ s, in which, a violent pool of boiling water accompanied by the generation of hot steam is observed (see Movie S1, Supporting Information). In Figure 5b, drops of water are placed onto the heater surface. At $T_s = 450$ °C, the Leidenfrost effect is clearly shown; also see Movie S2 (Supporting Information). The drops evaporate eventually at all the temperatures of 250, 350, and 450 °C, corresponding to the applied voltages of 0.5, 0.65, and 0.75 V, respectively.

To demonstrate the suitability of the supersonic spray method for coating complex 3D surfaces, a replica of the Jeju's Dol Hareubang statue was tested as a substrate on which the Cu–Ni particles were supersonically sprayed. Figure 5c shows the photograph of the Hareubang statue coated with Cu–Ni particles while the inset shows that of the noncoated statue. The hardness of the statue surface was high enough to prevent chipping by the impact of the supersonic particles. After spraying the Cu–Ni particles on the surfaces, a couple of electrodes were connected at the back end of the statue to provide an electric current. The trace of one electrode appears at the bottom right of the statue. When a voltage of 2 V (the maximum achievable voltage in this experiment) is applied with the corresponding current value of 30 A, the statue begins to heat up and reaches $T_s = 114$ °C within 30 s, as shown in the IR image in Figure 5d. Interestingly, the voltage level used here (2 V) is higher than that used in the previous cases, indicating that a larger surface curvature results in greater heat losses, and thus requires a higher voltage supply to keep it hot.

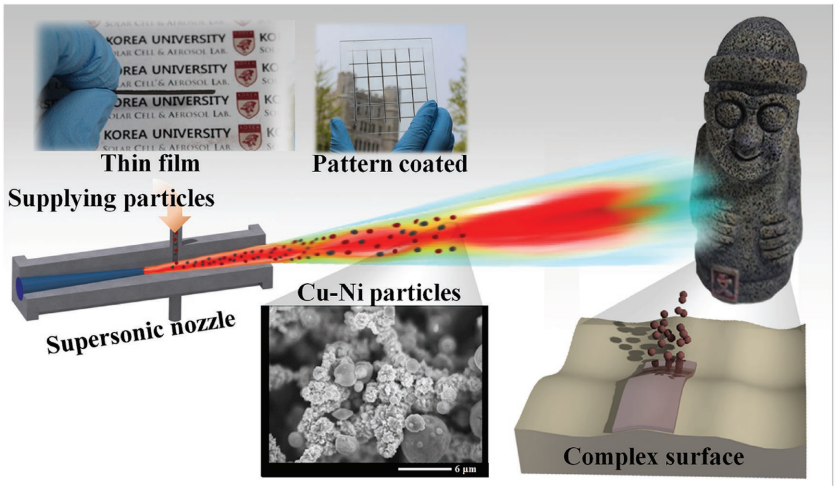

Figure 6. Schematic of supersonic cold-spray deposition. Middle bottom inset: SEM image of a Cu–Ni mixture before deposition onto the complex surfaces of the Jeju's Dol Hareubang statue replica. Top insets: 2D Cu–Ni thin film and patterned 1D Cu–Ni crossbars on a glass substrate, fabricated using the supersonic spraying technique.

3. Conclusions

Cu and Ni microparticles were supersonically sprayed onto various substrates of complex shapes forming a film heater that can reach extreme temperatures of about 1000 °C. The heater was reliable and revealed significant thermal stability for many cycles. The heater is bendable and patternable on complex 3D surfaces. Owing to the rapid increase to extreme temperature using ≈100 W of power supply, these film heaters hold great promise for various industrial applications that require moderate bendability, patternability, and transparency. An analytical model that accounted for the heat losses due to both convection and radiation was developed and the surface temperatures of the heaters fabricated at different Cu–Ni compositions and film thicknesses were accurately predicted.

4. Experimental Section

Figure 6 describes the supersonic cold-spray deposition of Cu–Ni particles. The Cu–Ni powder (Alfa Aesar, 99.99%) was fed through the diverging section of a supersonic Laval nozzle and entrained abruptly by a supersonic air stream. Owing to the small size of the particles, they quickly reach the supersonic velocity of the air stream. When they collide with the complex-shaped substrate, they are flattened by the direct conversion of the kinetic energy of impact into the energy of elastic-plastic deformation, which also promotes in situ sintering. This is followed by energy dissipation, finally leading to the deposition of the Cu–Ni film. The film thickness can be controlled by the number of nozzle sweeps (N). The supersonic gas velocity is set by the upstream chamber pressure, $P_0 = 4$ bar and the air temperature, $450 \leq T_0 \leq 650$ °C (see Table S1, Supporting Information), yielding an isentropic air velocity of 690–780 m s^{-1}. The Stokes number of the Cu–Ni particles is small ($0.02 < \mathrm{Stk} < 1.75$), based on the average particle size shown in Figure 1. Therefore, the small Stokes number facilitates their abrupt entrainment by the gas flow.[46,47] The cold spraying deposition process was described in detail in previous works.[44,48,49]

The surface morphologies and the elemental maps of the fabricated films were obtained using a field-emission scanning electron microscope (FE-SEM, S-5000, Hitachi, Ltd.) and a TEM (JEM 2100F, JEOL Inc.). The TEM sample was prepared using FIB milling. 3D images were obtained using an optical surface profiler (Wyko NT1100, Veeco) to estimate the roughness of the fabricated films. The current–voltage curves were measured using a current meter and voltmeter (3288, Digital Hitester 3256, HIOKI). Crystallinity and crystal phase were assessed using powder XRD (SmartLab, Rigaku, JAPAN) across a range of $30° < 2\theta < 80°$.

Supporting Information

Supporting Information is available from the Wiley Online Library or from the author.

Acknowledgements

J.-G.L. and D.-Y.K. contributed equally to this work. This work was supported by the Global Frontier Program through the Global Frontier Hybrid Interface Materials (GFHIM) of the National Research Foundation of Korea (NRF) funded by the Ministry of Science, ICT & Future Planning (2013M3A6B1078879). This research was supported by the Technology Development Program to Solve Climate Changes of NRF-2016M1A2A2936760. S. S. Yoon expresses his appreciation to the Vice Deanship of Scientific Research chairs at King Saud University.

Keywords

conducting films, convective and radiative heat transfer, copper–nickel heater, supersonic spray coating

Received: January 19, 2017
Revised: February 26, 2017
Published online:

[1] S. Thiriat, *US Patent 6341554 B2* **2002**.
[2] T. Itoh, M. Sakamoto, *US Patent 4455479 A* **1984**.
[3] J. C. Fan, F. J. Bachner, *Appl. Opt.* **1976**, *15*, 1012.
[4] K. Nishio, T. Sei, T. Tsuchiya, *J. Mater. Sci.* **1996**, *31*, 1761.
[5] M. Alam, D. Cameron, *Thin Solid Films* **2000**, *377*, 455.
[6] D. M. Mattox, *Thin Solid Films* **1991**, *204*, 25.
[7] I. Hamberg, C. G. Granqvist, *J. Appl. Phys.* **1986**, *60*, R123.
[8] S.-S. Kim, S.-Y. Choi, C.-G. Park, H.-W. Jin, *Thin Solid Films* **1999**, *347*, 155.
[9] G. Leftheriotis, S. Papaefthimiou, P. Yianoulis, *Solid State Ionics* **2000**, *136*, 655.
[10] M. Smyth, P. Eames, B. Norton, *Sol. Energy* **2001**, *70*, 391.
[11] A. Du Pasquier, H. E. Unalan, A. Kanwal, S. Miller, M. Chhowalla, *Appl. Phys. Lett.* **2005**, *87*, 203511.
[12] C. D. Williams, R. O. Robles, M. Zhang, S. Li, R. H. Baughman, A. A. Zakhidov, *Appl. Phys. Lett.* **2008**, *93*, 183506.
[13] C. Aguirre, C. Ternon, M. Paillet, P. Desjardins, R. Martel, *Nano Lett.* **2009**, *9*, 1457.
[14] K. Im, K. Cho, J. Kim, S. Kim, *Thin Solid Films* **2010**, *518*, 3960.
[15] H.-S. Jang, S. K. Jeon, S. H. Nahm, *Carbon* **2011**, *49*, 111.
[16] Y. H. Yoon, J. W. Song, D. Kim, J. Kim, J. K. Park, S. K. Oh, C. S. Han, *Adv. Mater.* **2007**, *19*, 4284.
[17] D. Jung, D. Kim, K. H. Lee, L. J. Overzet, G. S. Lee, *Sens. Actuators, A* **2013**, *199*, 176.
[18] D. Kim, H.-C. Lee, J. Y. Woo, C.-S. Han, *J. Phys. Chem. C* **2010**, *114*, 5817.
[19] J. Kang, H. Kim, K. S. Kim, S.-K. Lee, S. Bae, J.-H. Ahn, Y.-J. Kim, J.-B. Choi, B. H. Hong, *Nano Lett.* **2011**, *11*, 5154.
[20] D. Sui, Y. Huang, L. Huang, J. Liang, Y. Ma, Y. Chen, *Small* **2011**, *7*, 3186.
[21] J. J. Bae, S. C. Lim, G. H. Han, Y. W. Jo, D. L. Doung, E. S. Kim, S. J. Chae, T. Q. Huy, N. Van Luan, Y. H. Lee, *Adv. Funct. Mater.* **2012**, *22*, 4819.
[22] T. Kim, Y. W. Kim, H. S. Lee, H. Kim, W. S. Yang, K. S. Suh, *Adv. Funct. Mater.* **2013**, *23*, 1250.
[23] R. Gupta, K. Rao, K. Srivastava, A. Kumar, S. Kiruthika, G. U. Kulkarni, *ACS Appl. Mater. Interfaces* **2014**, *6*, 13688.
[24] P.-C. Hsu, X. Liu, C. Liu, X. Xie, H. R. Lee, A. J. Welch, T. Zhao, Y. Cui, *Nano Lett.* **2014**, *15*, 365.
[25] S. Sorel, D. Bellet, J. N. Coleman, *ACS Nano* **2014**, *8*, 4805.
[26] H.-G. Cheong, D.-W. Song, J.-W. Park, *Microelectron. Eng.* **2015**, *146*, 11.
[27] S. Hong, H. Lee, J. Lee, J. Kwon, S. Han, Y. D. Suh, H. Cho, J. Shin, J. Yeo, S. H. Ko, *Adv. Mater.* **2015**, *27*, 4744.
[28] Q. Huang, W. Shen, X. Fang, G. Chen, J. Guo, W. Xu, R. Tan, W. Song, *RSC Adv.* **2015**, *5*, 45836.
[29] N. Kwon, K. Kim, J. Heo, I. Yi, I. Chung, *Nanotechnology* **2014**, *25*, 265702.
[30] B. Seong, H. Yoo, V. D. Nguyen, Y. Jang, C. Ryu, D. Byun, *J. Micromech. Microeng.* **2014**, *24*, 097002.
[31] H.-J. Kim, Y. Kim, J.-H. Jeong, J.-H. Choi, J. Lee, D.-G. Choi, *J. Mater. Chem. A* **2015**, *3*, 16621.
[32] A. Khan, S. Lee, T. Jang, Z. Xiong, C. Zhang, J. Tang, L. J. Guo, W. D. Li, *Small* **2016**, *12*, 3021.

[33] P.-C. Hsu, S. Wang, H. Wu, V. K. Narasimhan, D. Kong, H. R. Lee, Y. Cui, *Nat. Commun.* **2013**, *4*, 2522.
[34] S. Han, S. Hong, J. Yeo, D. Kim, B. Kang, M. Y. Yang, S. H. Ko, *Adv. Mater.* **2015**, *27*, 6397.
[35] Y. D. Suh, J. Jung, H. Lee, J. Yeo, S. Hong, P. Lee, D. Lee, S. H. Ko, *J. Mater. Chem. C* **2017**, *5*, 791.
[36] J. Kwon, H. Cho, Y. D. Suh, J. Lee, H. Lee, J. Jung, D. Kim, D. Lee, S. Hong, S. H. Ko, *Adv. Mater. Technol.* **2017**, *2*, 1600222.
[37] B. Kang, S. Han, J. Kim, S. Ko, M. Yang, *J. Phys. Chem. C* **2011**, *115*, 23664.
[38] P.-H. Wang, S.-P. Chen, C.-H. Su, Y.-C. Liao, *RSC Adv.* **2015**, *5*, 98412.
[39] X. Zhang, X. Yan, J. Chen, J. Zhao, *Carbon* **2014**, *69*, 437.
[40] J.-G. Lee, D.-Y. Kim, B. N. Joshi, J.-H. Lee, T.-K. Lee, J.-S. Kim, D.-H. Yang, W.-Y. Kim, S. S. Al-Deyab, S. S. Yoon, *J. Therm. Spray Technol.* **2016**, *25*, 763.
[41] Y. Yamada, H. Sakate, F. Sakuma, A. Ono, *Metrologia* **2001**, *38*, 213.
[42] M. Sundberg, G. Malmqvist, A. Magnusson, T. El-Raghy, *Ceram. Int.* **2004**, *30*, 1899.
[43] J. Kang, Y. Jang, Y. Kim, S.-H. Cho, J. Suhr, B. H. Hong, J.-B. Choi, D. Byun, *Nanoscale* **2015**, *7*, 6567.
[44] J.-G. Lee, D.-Y. Kim, B. Kang, D. Kim, H.-E. Song, J. Kim, W. Jung, D. Lee, S. S. Al-Deyab, S. C. James, S. S. Yoon, *Acta Mater.* **2015**, *93*, 156.
[45] B. E. Meserve, *Fundamental Concepts of Algebra*, Dover Publ., New York, USA, **1982**.
[46] M.-W. Lee, J.-J. Park, D.-Y. Kim, S. S. Yoon, H. Y. Kim, D. Kim, S. C. James, S. Chandra, T. Coyle, J. Ryu, *J. Aerosol Sci.* **2011**, *42*, 771.
[47] M.-W. Lee, J.-J. Park, D.-Y. Kim, S. S. Yoon, H.-Y. Kim, S. C. James, S. Chandra, T. Coyle, *J. Therm. Spray Technol.* **2011**, *20*, 1085.
[48] J.-G. Lee, D.-Y. Kim, M. G. Mali, S. S. Al-Deyab, M. T. Swihart, S. S. Yoon, *Nanoscale* **2015**, *7*, 19027.
[49] D. Y. Kim, S. Sinha-Ray, J. J. Park, J. G. Lee, Y. H. Cha, S. H. Bae, J. H. Ahn, Y. C. Jung, S. M. Kim, A. L. Yarin, S. S. Yoon, *Adv. Funct. Mater.* **2014**, *24*, 4986.

